Fusion Engineering and Design 227 (2026) 115711

Contents lists available at ScienceDirect

Fusion Engineering and Design

journal homepage: www.elsevier.com/locate/fusengdes

Simulation of water activation in the KATANA activation loop of the TRIGA reactor

Primož Lesjak [a,b], Aljaž Čufar [a], Domen Kotnik [a], Julijan Peric [a,b], Marco De Pietri [c], Luka Snoj [a,b,*]

[a] Reactor Physics Department, "Jožef Stefan" Institute, Jamova cesta 39, Ljubljana, 1000, Slovenia
[b] Faculty of Mathematics and Physics, University of Ljubljana, Jadranska ulica 19, Ljubljana, 1000, Slovenia
[c] MIT, Plasma Science and Fusion Center (PSFC), 77 Massachusetts Avenue, Cambridge, 02139, United States

ARTICLE INFO

Keywords:
Water activation
KATANA
JSI TRIGA
FLUNED
Fusion
ITER

ABSTRACT

Water is widely used as a coolant in both fission and fusion nuclear reactors. However, when exposed to neutrons, it becomes activated and can turn into a significant radiation source especially in fusion reactors operating with deuterium–tritium plasma. This effect influences reactor design and requires accurate modeling to ensure safe and reliable operation. During the development of the ITER fusion reactor, methods and codes were created to simulate the process of water activation and its flow through the cooling system. However, lack of relevant experiments needed for experimental validation of these codes was highlighted.

In 2024, the KATANA water activation facility began operating at the TRIGA Mark II reactor at the Jožef Stefan Institute with the aim to improve understanding of water activation and to validate computational tools used for simulating it.

This paper presents an analysis of water activation in the KATANA loop using the open-source FLUNED code, which integrates fluid dynamics with neutron and gamma-ray transport simulations. The analysis focuses on activation calculations based on the latest loop design. Additionally, we examine how uncertainties in some of the main input parameters, i.e. flow rate and the total volume of the loop components, influence the overall uncertainty in the determined activity of water.

1. Introduction

Water is the most common coolant used in fission reactors and will also be used in large fusion reactors like the ITER tokamak [1–5]. Both in the core of fission reactors and during the cooling of fusion reactor components, water is exposed to neutrons. This exposure leads to the activation of water, resulting in the production of radioactive isotopes. As these activation products undergo radioactive decay within the cooling loop, they emit high-energy gamma rays and neutrons. Since the cooling circuit typically extends beyond the biological shield, radiation can affect various parts of the reactor complex including sensitive components and personnel. Consequently, shielding of the cooling loop is necessary to protect electronic systems, instruments, superconducting coils, and personnel. To design effective shielding and ensure reactor safety, it is essential to develop predictive tools capable of accurately modeling the radiation dose field resulting from activated water. In addition, modeling and understanding water activation can serve as a valuable diagnostic tool, providing insights into reactor operating conditions [6–8].

Quantifying the spatial distribution of radionuclide activity is a complex process that requires the coupling of fluid dynamics and neutron transport simulations. The complexity of these calculations depends on factors such as coolant type, velocity fields, and irradiation conditions. In scenarios where water flows rapidly through pipe circuits, modeling is simplified. Under fully developed turbulent flow conditions, the assumption of a uniform velocity distribution provides an effective approximation for estimating radionuclide production and decay [9]. However, deviations from this assumption due to complex geometries or non-uniform flow patterns can introduce significant inaccuracies in activation calculations. To enhance the accuracy of water activation studies in complex flow conditions, some research groups have developed methodologies that integrate Computational Fluid Dynamics (CFD) codes and neutron transport codes. One such code is the open-source FLUNED [9], while another is RSTM code [10].

Newly developed computational models must be validated against experimental data. A facility designed to run such experiments named KATANA [11,12] was constructed in 2023 and is operating at the IJS

* Corresponding author at: Reactor Physics Department, "Jožef Stefan" Institute, Jamova cesta 39, Ljubljana, 1000, Slovenia.
E-mail address: luka.snoj@ijs.si (L. Snoj).

https://doi.org/10.1016/j.fusengdes.2026.115711
Received 6 October 2025; Received in revised form 16 February 2026; Accepted 7 March 2026
Available online 16 March 2026

Table 1
Activation of oxygen isotopes in water and associated decay characteristics.

Reaction	Natural abundance (%)	$t_{1/2}$ [s]	Main decay products
^{16}O(n, p)^{16}N	99.76	7.13	6.129 MeV γ (67%) 7.115 MeV γ (5%)
^{17}O(n, p)^{17}N	0.04	4.17	0.383 MeV n (35%) 1.171 MeV n (53%)
^{18}O(n, γ)^{19}O	0.20	26.9	0.197 MeV γ (63%) 1.357 MeV γ (33%)

TRIGA [13–17] research reactor. This facility utilizes neutrons from the fission reactor to activate recirculating water in a closed-loop, which then serves as a well defined gamma radiation source with photon energies ranging from 6 MeV to 7 MeV. This setup enables a variety of experiments related to water activation [18,19].

The objective of this paper is to present the results of activity calculations in KATANA using the latest experimental setup, as described in [11], using FLUNED code. A quantitative uncertainty analysis of the calculated water activity is also presented, based on the flow rate and loop volume uncertainties reported in [20].

2. Water activation

When water is exposed to neutrons, oxygen nuclei undergo activation, resulting in the formation of radioactive oxygen and nitrogen isotopes through ^{16}O(n, p)^{16}N, ^{17}O(n, p)^{17}N, and ^{18}O(n, γ)^{19}O reactions. Furthermore, hydrogen, present as both ^{1}H and ^{2}H, can also be activated. In particular, neutron capture by ^{2}H leads to the formation of tritium (^{3}H). However, due to its much longer half-life and negligible gamma emission during decay, the contribution of ^{3}H is often considered insignificant and is therefore neglected [3]. In this study, we also consider only the activation of the three oxygen isotopes.

Table 1 summarizes the dominant activation reactions for each oxygen isotope, together with the resulting activation product, its half-life, and major decay emissions with branching ratios. The most important activated nuclide is ^{16}N, primarily due to the high natural abundance of ^{16}O, the relatively high activation cross section and the emission of high-energy gamma rays during its decay. The decay of ^{17}N is important as it produces neutrons, which can activate the reactor components surrounding the cooling system and can lead to secondary gamma radiation in parts of the reactor where activation of components would otherwise be negligible. Decay of ^{19}O also emits gamma rays, though at lower energies compared to those of ^{16}N. In contrast to ^{16}N and ^{17}N, which are formed through threshold reactions, ^{19}O can already be produced by thermal neutron capture. Since all water activation products have relatively short half-lives, their relevance is primarily limited to periods of reactor operation and a short amount of time right after the reactor is shut down.

3. Computational model

The activation process depends on the flow dynamics, geometry, and distribution of both neutron flux and spectrum, requiring appropriate modeling techniques to ensure accurate predictions. In this paper, a combination of different approaches is used to calculate water activation.

The first approach is well-suited for scenarios where water flows rapidly through simple geometries. In such cases, the flow typically exhibits fully developed turbulent behavior, allowing the assumption of a uniform velocity vector field. This assumption simplifies the calculation of radionuclide formation and decay.

When considering only the transport and decay of an activated product, without additional activation, the uniform velocity approximation allows us to express the activity of water at the outlet of a pipe in relation to its activity at the inlet as:

$$a_o = a_i e^{-t_{res}\lambda}, \tag{1}$$

where a_o is the outlet radioisotope activity, a_i is the inlet activity, λ represents the decay constant of the activated product, and t_{res} is the total time a fluid spends inside the pipe, also called the residence time. This can be calculated as

$$t_{res} = \frac{V}{\Phi_V}, \tag{2}$$

where V is the volume of water in the pipe section, and Φ_V is the flow rate of the water.

However, in cases where the water flow does not exhibit fully developed turbulence or where the geometry deviates from pipe configurations, relying solely on uniform velocity methods can lead to significant inaccuracies in fluid activation. In such situations, incorporating computational fluid dynamics (CFD) analysis becomes essential.

In our study, we utilized the FLUNED code, whose methodology and operation are detailed in [9]. The program takes as input the velocity profile obtained from CFD simulations and the reaction rate profile. As output, it provides distribution of activation products, which is then used to generate a Common Decay Gamma Source (CDGS) [21] file describing the spatial and spectral distribution of the resulting gamma-ray and neutron sources. This file is subsequently used in Monte Carlo particle transport simulation to simulate the corresponding dose fields.

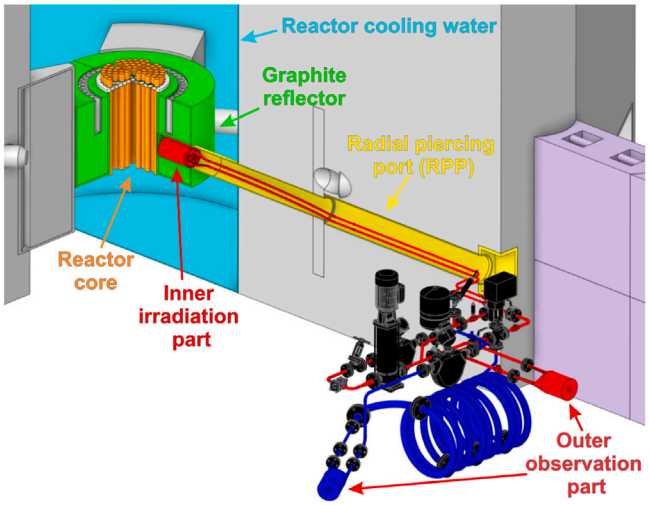

Fig. 1. Schematic diagram of the KATANA water activation loop at the JSI TRIGA reactor [11].

4. Workflow

Our calculations were performed for the case of the KATANA water activation loop, depicted in Fig. 1. In this activation loop, water circulates in a closed cycle. Activation occurs in the inner irradiation part, where the water is exposed to neutrons originating from the core of the TRIGA reactor. The vast majority of activation takes place in a specially designed, snail-like component, depicted in Fig. 2 positioned near the reactor core. This component is engineered to maximize the water residence time near the reactor core, ensuring that it undergoes a high level of activation.

After activation, the water is transported to the outer observation section of the loop. The system includes two distinct configurations of the outer loop: Configuration 1, which represents the short loop (red), and Configuration 2, which represents the long loop (blue). The long loop features a significantly larger volume, allowing for longer

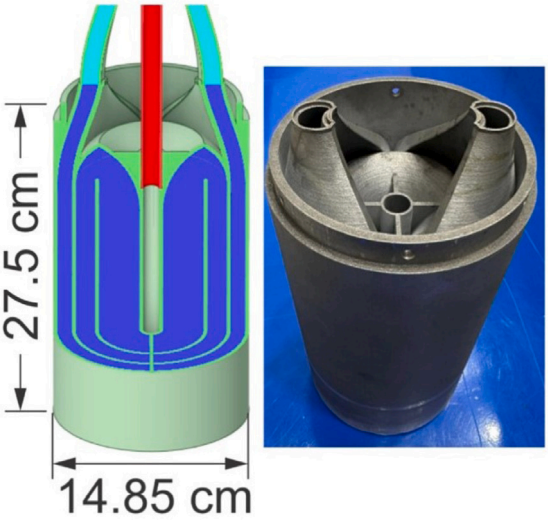

Fig. 2. Schematic of the detailed model of the complex irradiation part, i.e. the inner Snail, and the manufactured part (completely 3D-printed from aluminium). [11].

Table 2
Loop segment volumes for both configurations.

Configuration	Config. 1	Config. 2
Volume from IRR to OBS [l]	0.6	23.1
Volume from OBS to IRR [l]	6.2	6.4

transport times and different activity profiles. At the end of both loops, there is another snail-like component, i.e. outer observation part, similar to the one in the inner section, i.e. inner irradiation part. The volumes of the sections between the irradiation (IRR) and observation parts (OBS) of each loop configuration are shown in Table 2. These volumes are defined as the total amount of water contained within the pipes and associated instrumentation between the outlet of the inner irradiation snail and the inlet of the outer observation snail, and vice versa.

In the IRR-to-OBS direction, the volume contribution comes almost exclusively from the piping. Conversely, in the OBS-to-IRR direction, components such as the pump contribute significantly to the total volume.

In this study, we focused on a steady state case where the water flow in the loop is constant, the reactor operates at steady-state power of 250 kW, and both water pump and reactor have been operating for a sufficiently long time to reach saturation activity within the loop. The power of the JSI TRIGA reactor is monitored by using the so-called linear channel featuring compensated ionization chamber. The absolute calibration of the linear channel is performed by the calorimetric method described in [22,23]. The calibration is done after every major change in the core or at least once a year. The water flow rate ranged from near zero to approximately 0.68 l/s, corresponding to Reynolds numbers between 8×10^3 and 1.1×10^5, indicative of turbulent flow conditions.

Our starting point for activity calculations was a CAD model of the KATANA water activation loop. The first step involved simplifying this model by replacing all complex supporting components, such as pumps, flow meters, and sensors, with pipes of equivalent water volume. In these pipes, the uniform velocity approximation was applied. Since activation in the pipes is negligible in our case, the transport of activated products was described using Eq. (1). It should be noted that water flow in components such as pumps is generally non-uniform. However, due to the lack of detailed models for these components and the complexity of simulations even with such models, the uniform velocity approximation was used as the most feasible approach for describing water flow in this context. In future experiments, it is possible to deploy detectors at the outlet/inlet of this complex structural component to directly measure activity and verify the rationality of the above hypothesis.

In components where water flow does not exhibit fully developed turbulence or where activation is the most significant and where detectors are placed near large volumes of activated water, i.e. the inner and outer snail, FLUNED was used. CFD simulations were performed using the open-source software OpenFOAM [24], while reaction rates were calculated with MCNP [25].

Since the KATANA water activation loop is a closed system, the saturation activity value is not reached instantly after the activation process begins. Instead, it gradually increases with each water circulation until saturation is achieved. The saturation concentration could be determined using an iterative process; however, this approach would require multiple FLUNED simulations, which are computationally expensive.

The use of saturated activity represents a specific operational regime of the water activation loop and is applicable only when the neutron source can be considered quasi-steady-state over a sufficiently long irradiation period. For activation dominated by the decay of ^{16}N, saturation is reached after several isotope half-lives, corresponding to irradiation times of approximately 20–35 s under constant neutron flux conditions. This makes saturated activity measurements well suited to steady-state neutron sources, such as fission reactors, and to long-pulse operation scenarios anticipated during the power production phases of fusion devices. In contrast, for transient scenarios, the KATANA water activation system can be operated in a time-resolved mode, where the transient evolution of the activation signal is used instead of the saturation value [20].

The saturated activity approach presented here therefore serves primarily as a validation step for the activation transport model and system characterization, forming a basis for subsequent application to transient irradiation scenarios.

As an alternative, saturation activity can be estimated analytically by describing the system with a simplified schematic, shown in Fig. 3. In this representation, the loop is divided into its key components: pipes, outer, and inner snail. Each component influences the activity of the circulating water in a specific way.

In the pipes, where a constant velocity is assumed, the reduction in activity is described by exponential decay $e^{-\lambda t_V}$, where t_V is the total time the water spends in the pipes per cycle. This consists of two parts: t_o, the time from the inner snail to the outer snail, and t_i, the time from the outer snail back to the inner snail, giving $t_V = t_o + t_i$.

In an outer snail, the situation is more complicated, as different parts of the liquid have different trajectories. Nevertheless, the influence of the outer observation snail on the activity at a given speed can be described as multiplication by a constant C, which represents the ratio of the specific coolant activity at the outlet to that at the inlet. The inner irradiation snail introduces additional complexity, as it involves simultaneous activation and decay. Its effect is modeled by multiplying the inlet activity by a decay factor B and adding a constant a, which accounts for the activation contribution.

The constants C and B are determined by assigning a fixed reference activity at the coolant inlet of the inner and outer snails and then performing simulations with FLUNED to calculate the outlet-to-inlet activity ratio. The constant a is determined from a case where the coolant entering the inner irradiation snail has zero initial activity but is exposed to radiation, making a equal to the resulting outlet activity.

Using this analytical model, the saturation activity at the outlet of the inner snail can be determined by:

$$A_{io} = \frac{a}{1 - B \cdot C \cdot e^{-\lambda t_V}}. \tag{3}$$

The saturation activity at the inlet of the inner snail is then given by:

$$A_{ii} = A_{io} e^{-\lambda t_V} C, \tag{4}$$

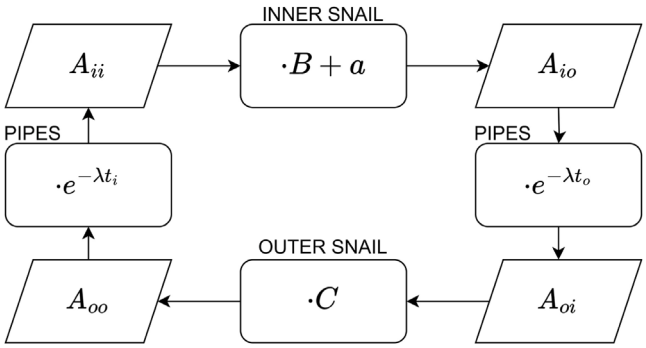

Fig. 3. Simplified schematic of the activation loop.

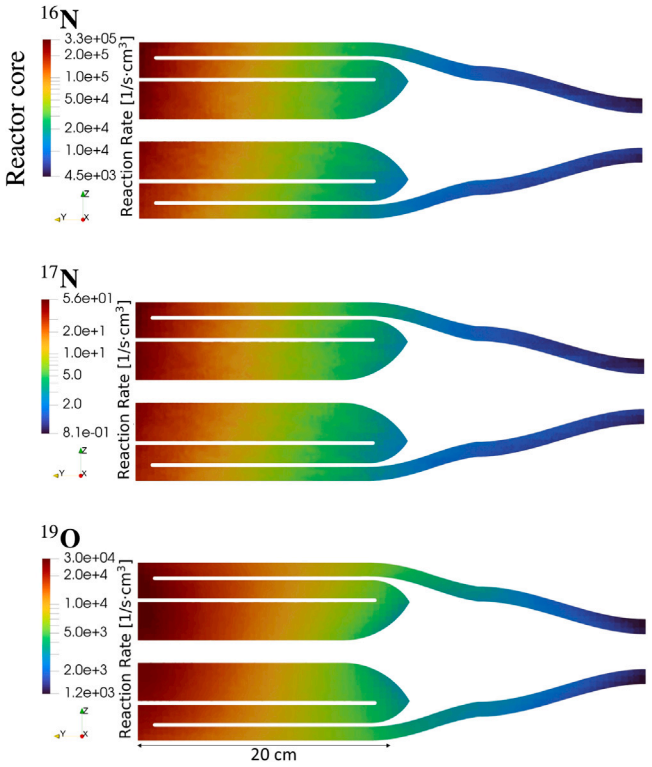

Fig. 4. Reaction rate profiles for the generated isotopes along the cross-section of the inner irradiation snail, normalized to the full reactor power of 250 kW.

while the saturation activity at the inlet of the outer snail is calculated as:

$$A_{oi} = A_{io} e^{-\lambda t_o}. \tag{5}$$

5. Activity calculations

5.1. Reaction rates

The reaction rates (RR) within the inner irradiation snail were calculated using MCNP5 v1.6 with the Oak Ridge National Laboratory Transformative Neutronics (ORNL-TN) upgrade [26]. For variance reduction, ADVANTG v3.20 [27] was used. MCNP simulations were performed with the ENDF ENDF/B-VIII.0 nuclear data library [28], whereas for ADVANTG calculations the FENDL-3.1 [29] nuclear cross section library with a 46-group neutron and 21-group gamma energy structure was used. The conversion of a simplified CAD model of the inner snail into MCNP geometry was done using the open source code

Table 3
FLUNED factors (B, a, C_s, C_l) for two flow rates.

Flow [l/S]	Activation product	a [Bq/m^3]	B	C_s	C_l
0.05	^{16}N	5.71E+10	6.0E−3	6.1E−3	6.4E−3
	^{17}N	8.07E+6	2.2E−4	2.3E−4	2.6E−4
	^{19}O	8.84E+9	0.23	0.23	0.23
0.5	^{16}N	3.19E+10	0.57	0.57	0.57
	^{17}N	7.77E+6	0.39	0.39	0.39
	^{19}O	1.70E+9	0.86	0.86	0.86

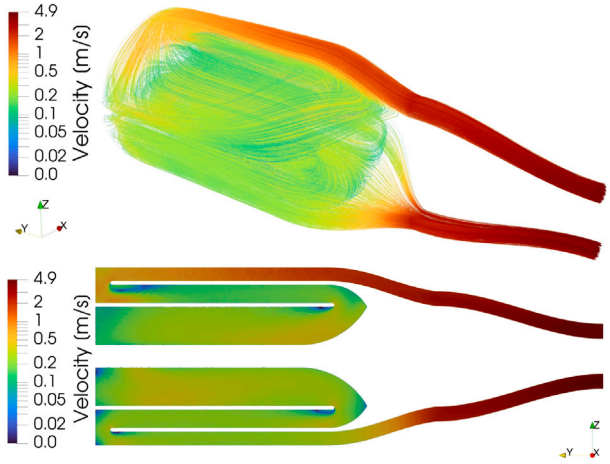

Fig. 5. Velocity profiles along streamlines and across the cross-section of the inner irradiation snail at a flow rate of 1 l/s.

GEOUNED [30]. A more detailed description of the computational methodology is provided in [11]. The results of the reaction rate calculations are shown in Fig. 4.

5.2. Velocity profile

Velocity fields of water within the inner and outer snail geometries were calculated using the open-source CFD software OpenFOAM v12 for flow rates ranging from 0.05 to 1.00 l/s, with increments of 0.05 l/s. The turbulence model used in the CFD calculations was the k-epsilon (k-ϵ) turbulence model. Fig. 5 shows the velocity profiles along the streamlines and along the cross section of the inner irradiation snail at a flow rate of 1 l/s. Due to the geometric similarities between the inner and outer snail, the velocity profiles in the outer snail are also very similar.

5.3. Distribution of activation products

Combining the information about reaction rates and velocity profiles using FLUNED, we first calculated the parameters B, C, and a for each flow rate. The results for two flow rates are summarized in Table 3. In the table, C_s denotes the radiation snail factor for the short loop, while C_l represents the corresponding factor for the long loop. Using Eq. (2) and the volumes from Table 2, the residence times t_o, t_i and t_V were then calculated. Based on Eqs. (4) and (5), we obtained the saturation values of the inlet activity. These values were used to rerun the FLUNED simulations, resulting in the distribution of activation products inside both the inner and outer snail. An example of the resulting distribution is shown in Fig. 6. Based on this calculated distribution, FLUNED automatically generates the source definition of gamma rays and neutrons in CDGS format, which can be directly used as input for a modified version of MCNP.

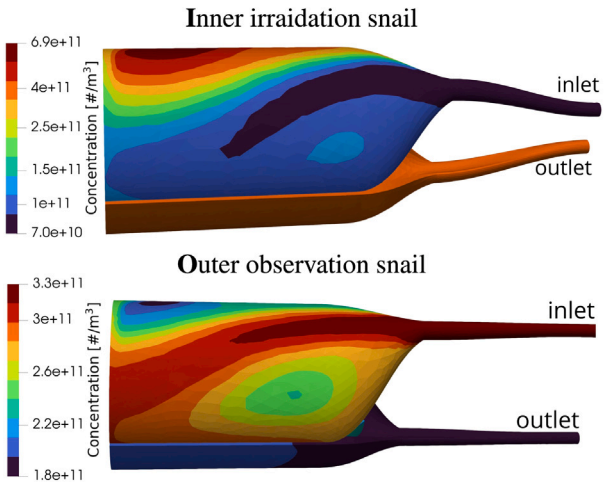

Fig. 6. Spatial distribution of ^{16}N within the inner and outer snail of the short loop at a flow rate of 0.5 l/s.

5.4. Activity dependence on flow

As the flow rate in the loop can be varied from near zero up to approximately 0.68 l/s, we investigated how different flow rates affect the saturation activity of activation products inside the outer observation snail. To provide a clearer trend, we extended the calculations to include flow rates up to 1 l/s. We also looked at how the saturated specific activity at the inlet of the outer observation snail changes with flow rate. The results for the shorter loop are shown in Fig. 7.

It can be observed that as the flow rate in the loop increases, the specific activity at the inlet of the outer observation snail initially increases, reaches a maximum, and then begins to decline. Similarly, the total activity follows the same trend, but peaks at a higher flow rate and decreases more gradually. This behavior can be explained by the fact that, at higher flow rates, the drop in specific activity along the snail is less pronounced due to shorter residence times. As a result, the average specific activity and, consequently, the total activity inside the snail remains higher, even when the inlet-specific activity is already decreasing.

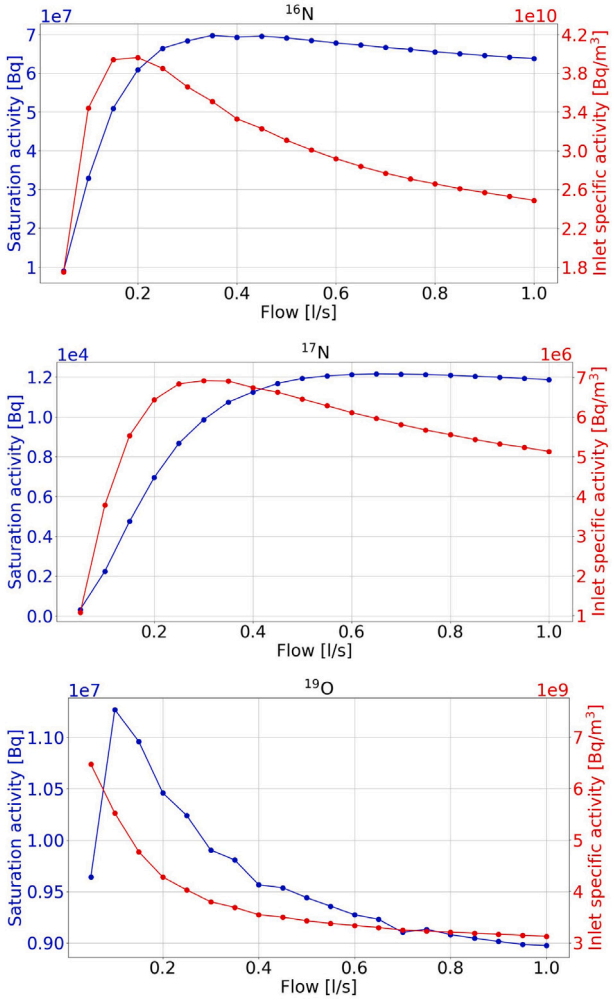

Fig. 7. Dependence of the activity within the outer observation snail and the specific activity at its entrance due to the decay of individual activation products as a function of the water flow in the short loop.

5.5. Calculation of dose rates

Based on the CDGS file generated by FLUNED, the dose rates around the outer observation snail were calculated using MCNP. An example of the dose field at a flow rate of 0.5 l/s is shown in Fig. 8. In these calculations, only the geometry of the snail and the water inside were modeled. For more realistic results, geometry based on an experimental setup should be added.

The dose rates within the central cavity of the outer observation snail, where detectors can be positioned, were also evaluated. The calculation domain is illustrated in Fig. 9. The domain was divided into thin slices along the snail's axis and the dose field was evaluated in each slice. An example of the resulting dose distribution for a specific flow rate and activation product is shown in Fig. 10. The shape of the dose field remains nearly identical for different flow rates. As shown, the dose rate is highest in the central region of the outer observation snail and gradually decreases toward the edges.

We also calculated the average dose rates within the defined region of the outer observation snail for different flow rates in the short loop. The results, presented in Fig. 11, show the dependence of the average gamma and neutron dose rates on the flow rate. The gamma dose field includes contributions from both ^{16}N and ^{19}O, while the neutron dose field originates from the decay of ^{17}N. A similar calculation for the long loop is shown in Fig. 12. In this case, the dose rates are significantly lower. At lower flow rates up to approximately 0.4 l/s, the gamma dose field is primarily dominated by contributions from ^{19}O. Therefore, operating the system at reduced flow rates in the long loop configuration is suitable for experiments aimed at studying ^{19}O contribution to the water activation.

5.6. Uncertainty of calculated activity due to uncertainty of loop volume and flow rate

Over the past year, the estimated total volume of the loop has been revised several times. The current best estimate is presented in Table 2. These updates are due to the difficulty in accurately determining the actual volume of water inside more complicated components, primarily the water pump. This volume uncertainty is particularly significant for the short loop, where the pump volume constitutes the majority of the total water volume outside the two snails.

Based on the latest measurements presented in [20], the uncertainty of the total volume is estimated to be 0.05 l, with the vast majority of the uncertainty originating from the pump volume. Using this value, we calculated the resulting uncertainty in the water activity inside the outer observation snail of the short loop. As shown in Fig. 13, the results demonstrate that across the entire operating range, the uncertainty in water activity caused by the volume uncertainty remains well below 1% for all activation products.

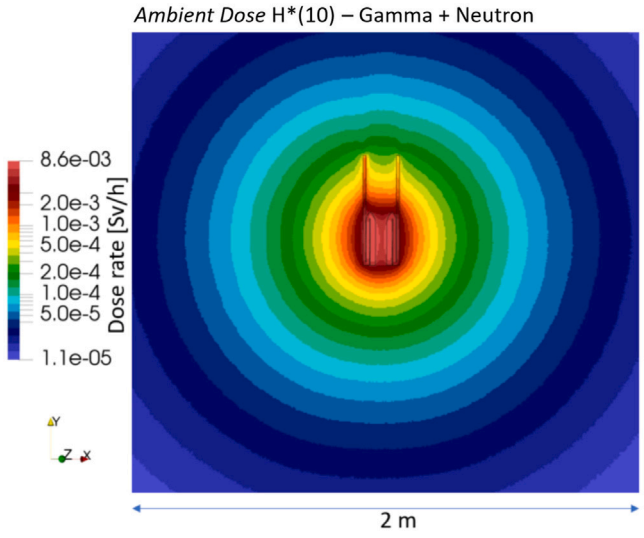

Fig. 8. Dose field in the vicinity of an outer observation snail at a flow rate of 0.5 l/s within a short loop.

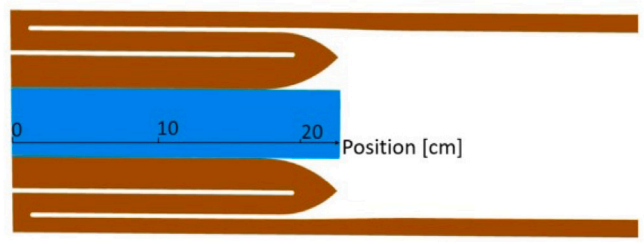

Fig. 9. Illustration of the dose calculation region (blue area) inside the outer observation snail.

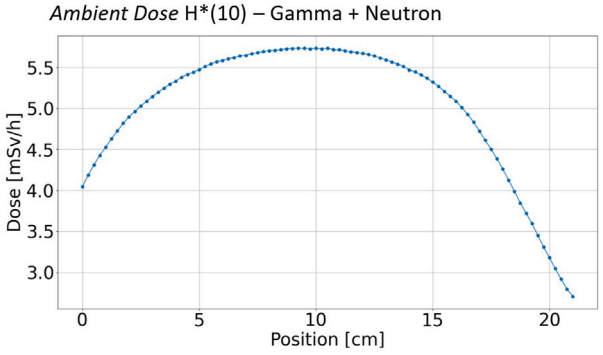

Fig. 10. Shape of the dose field within the outer observation snail at flow rate 0.5 l/s within a short loop.

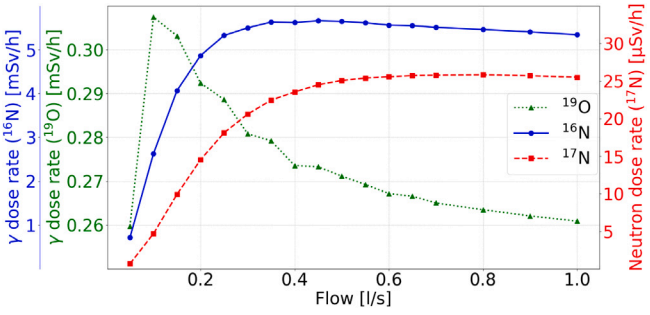

Fig. 11. Average dose field, calculated in the region marked in Fig. 9, as a function of the flow rate in the short loop.

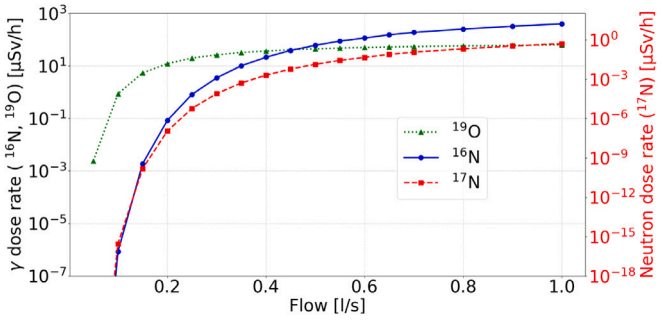

Fig. 12. Average dose field, calculated in the region marked in Fig. 9, as a function of the flow rate in the long loop.

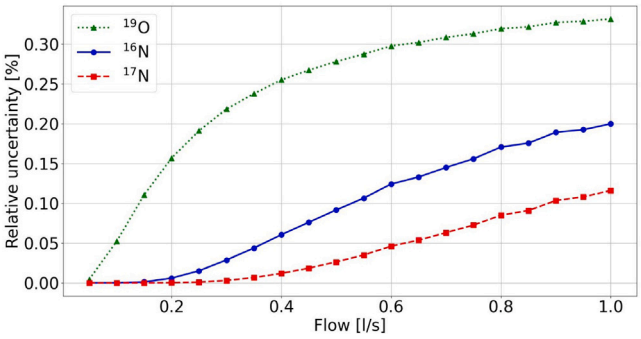

Fig. 13. Estimated relative uncertainty of water activity in the short loop due to a 0.05 l volume uncertainty, as a function of flow rate.

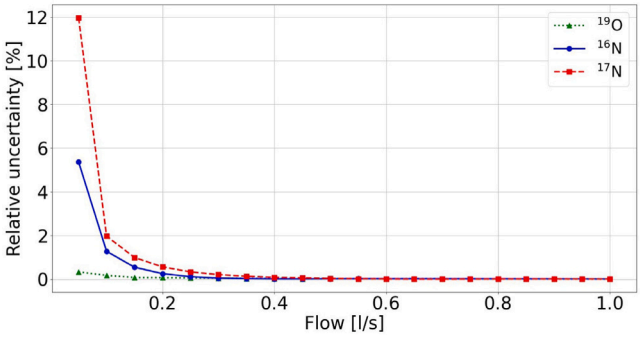

Fig. 14. Estimated relative uncertainty of water activity in the short loop due to a 0.001 l/s flow rate uncertainty, as a function of flow rate.

In addition to the volume uncertainty, the uncertainty in the flow rate of the loop also affects the accuracy of the activity calculations. According to [20], the uncertainty of the flow rate is estimated to be 0.001 l/s. Since the activity of water was calculated only at discrete flow rates, spaced by 0.05 l/s, the uncertainty was estimated by assuming a linear change in activity between these points. Based on this assumption, an approximate uncertainty evaluation was performed for a short loop, as shown in Fig. 14.

It can be seen that at lower flow rates, the uncertainty is more significant - particularly for the short-lived nuclides ^{16}N and ^{17}N, whose saturation activity changes rapidly in this low-flow regime. However, for flow rates commonly used in current experiments (that is, above 0.5 l/s), the uncertainty in activity due to flow rate variations remains well below 1%.

Conclusions

Activated cooling water can represent a challenge in design of fusion reactors as it can represent one of the more important sources of radiation far from fusion plasma, e.g. outside of the bioshield. Coupling of neutronics and thermohydraulics codes is required to accurately model this process.

In this paper we used FLUNED code to simulate water activity in KATANA activation loop. The activations of the oxygen isotopes ^{16}O, ^{17}O and ^{18}O and the decay of their activation products were taken into account: ^{16}N, ^{17}N and ^{19}O. For each of the se nuclides, the saturation activity was estimated at different flow rates and the dose fields were calculated.

At a TRIGA reactor power of 250 kW, the maximum saturation activity values achieved in the short loop were 7.1×10^7 Bq for ^{16}N at 0.5 l/s, 1.2×10^4 Bq for ^{17}N at 0.8 l/s, and 1.1×10^7 Bq for ^{19}O at 0.1 l/s. These activities correspond to gamma ray dose rates of 5.7 mSv/h for ^{16}N and 0.31 mSv/h for ^{19}O, and a neutron dose rate of 26 μSv/h for ^{17}N, all calculated inside the central cavity of the outer observation snail.

An uncertainty analysis was also carried out to assess the impact of two input parameters: the total water volume in the loop and the flow rate. Based on the latest measurements, a volume uncertainty of 0.05 l and a flow rate uncertainty of 0.001 l/s were assumed. The results show that for typical operating conditions (flow rates above 0.5 l/s), the resulting relative uncertainty in water activity in the outer observation snail of the short loop remains well below 1% for all activation products. This confirms that uncertainties in flow rate and volume have only a minor influence on the accuracy of the simulations and that the typical operational regime of KATANA is insensitive to minor changes in these operation parameters.

For future work, these simulation results can be directly compared with experimental measurements of water activity and dose rates, providing a valuable validation of the FLUNED code and enabling further refinement of simulation models.

CRediT authorship contribution statement

Primož Lesjak: Writing – original draft, Visualization, Validation, Methodology, Investigation, Formal analysis, Conceptualization. **Aljaž Čufar:** Writing – review & editing, Visualization, Supervision, Conceptualization. **Domen Kotnik:** Writing – review & editing, Funding acquisition, Conceptualization. **Julijan Peric:** Writing – review & editing, Conceptualization. **Marco De Pietri:** Writing – review & editing, Conceptualization. **Luka Snoj:** Writing – review & editing, Supervision, Funding acquisition, Conceptualization.

Declaration of competing interest

The authors declare that they have no known competing financial interests or personal relationships that could have appeared to influence the work reported in this paper.

Acknowledgments

This work has been carried out within the framework of the EUROfusion Consortium, funded by the European Union via the Euratom Research and Training Programme (Grant Agreement No 101052200 — EUROfusion). Views and opinions expressed are however those of the author(s) only and do not necessarily reflect those of the European Union or the European Commission. Neither the European Union nor the European Commission can be held responsible for them.

The authors acknowledge the financial support from the Slovenian Research Agency (research program No. P2-0073, project NC-0022).

Data availability

Data will be made available on request.

References

[1] ITER, 2024, https://www.iter.org/.(Accessed 29 July 2024).
[2] A. Zohar, A. Pungerčič, K. Ambrožič, V. Radulović, I. Lengar, L. Snoj, Analysis of irradiation experiments with activated water radiation source at the JSI TRIGA research reactor, Fusion Eng. Des. 161 (2020) http://dx.doi.org/10.1016/j.fusengdes.2020.111946.
[3] A. Žohar, L. Snoj, On the dose fields due to activated cooling water in nuclear facilities, Prog. Nucl. Energy 117 (2019) http://dx.doi.org/10.1016/j.pnucene.2019.103042.
[4] A. Žohar, I. Lengar, L. Snoj, Analysis of water activation in fusion and fission nuclear facilities, Fusion Eng. Des. 160 (2020) http://dx.doi.org/10.1016/j.fusengdes.2020.111828.
[5] V. Radulović, L. Snoja, et al., Preparation of a water activation experiment at JET to support ITER, Fusion Eng. Des. 169 (2021) 112410.
[6] J. Kaneko, Y. Uno, T. Nishitani, F. Maekawa, T. Tanaka, Y. Shibata, Y. Ikeda, H. Takeuchi, Technical feasibility study on a fusion power monitor based on activation of water flow, Rev. Sci. Instrum. 72 (2001) 809–813, http://dx.doi.org/10.1063/1.1320996.
[7] Y. Uno, J. Kaneko, T. Nishitani, F. Maekawa, T. Tanaka, S. Shibata, Y. Ikeda, V. Khripunov, C. Walker, K. Ebisawa, H. Takeuchi, Absolute measurement of D–t neutron flux with a monitor using activation of flowing water, Fusion Eng. Des. 56–57 (2001) 895–898, http://dx.doi.org/10.1016/S0920-3796(01)00373-8.
[8] T. Nishitani, M. Ishikawa, T. Kondoh, Y. Kusama, K. Asai, M. Sasao, Absolute neutron emission measurement in burning plasma experiments, AIP Conf. Proc. 988 (2008) 267–274, http://dx.doi.org/10.1063/1.2905079.
[9] M.D. Pietri, E. Rodríguez, R. Juárez, Development and validation in water of FLUNED, an open-source tool for fluid activation calculations, Comput. Phys. Comm. 291 (2023) http://dx.doi.org/10.1016/j.cpc.2023.108807.
[10] E. Masia, F. Cau, A. Kolsek, R. Pampin, M. Fabbri, L. Snoj, D. Kotnik, R. Villari, A. Portone, Application of the radio species transport model to the JSI water activation loop, Fusion Eng. Des. (2025) In review process.
[11] D. Kotnik, J. Peric, D. Govekar, L. Snoj, I. Lengar, KATANA - water activation facility at JSI TRIGA, part I: Final design and activity calculations, Nucl. Eng. Technol. 57 (3) (2025) 103233, http://dx.doi.org/10.1016/j.net.2024.09.036.
[12] D. Kotnik, A.K. Basavaraj, L. Snoj, I. Lengar, Design optimization of the closed-water activation loop at the JSI irradiation facility, Fusion Eng. Des. 193 (2023) 113632, http://dx.doi.org/10.1016/j.fusengdes.2023.113632.
[13] T. Goričanec, L. Snoj, K. Ambrožič, L. Barbot, L. Benedik, A. Bratkič, I. Capan, C. Reynard-Carette, V. Cindro, D. Čalič, C. Destouches, B. Geslot, A. Haghighat, R. Henry, M. Horvat, E.M. Huseynov, G. de Izarra, R. Jaćimović, A. Jazbec, I. Jenčič, et al., A half-century of nuclear research, education and training: Story of the JSI TRIGA reactor, Ann. Nucl. Energy 214 (2025) 111122, http://dx.doi.org/10.1016/j.anucene.2024.111122.
[14] I. Mele, M. Ravnik, A. Trkov, TRIGA mark II benchmark experiment; part I: Steady-state operation, Nucl. Technol. (United States) 105:1 (1993) URL https://www.osti.gov/biblio/5386395.
[15] R. Jeraj, T. Žagar, M. Ravnik, Monte Carlo simulation of the TRIGA mark II benchmark experiment with burned fuel, Nucl. Technol. 137 (3) (2002) 169–180, http://dx.doi.org/10.13182/NT02-A3266, arXiv:https://doi.org/10.13182/NT02-A3266.
[16] Ž. Štancar, L. Snoj, L. Barbot, Reaction rate distribution experiments at the Slovenian JSI TRIGA mark II research reactor, Int. Handb. Eval. React. Phys. Benchmark Exp. TRIGA-FUND-RESR-002 Paris (2017).
[17] G. Žerovnik, L. Snoj, A. Trkov, L. Barbot, D. Fourmentel, J.-F. Villard, Measurements of thermal power at the TRIGA mark II reactor in Ljubljana using multiple detectors, IEEE Trans. Nucl. Sci. 61 (5) (2014) 2527–2531.
[18] D. Kotnik, J. Peric, D. Govekar, L. Snoj, I. Lengar, KATANA - water activation facility at JSI TRIGA, part II: First experiments, Nucl. Eng. Technol. (2024) http://dx.doi.org/10.1016/j.net.2024.10.052.
[19] J. Peric, D. Kotnik, L. Snoj, V. Radulovic, Water activation experiment under fusion-relevant conditions at the JSI TRIGA research reactor KATANA: Neutron field measurement system, Fusion Eng. Des. (2025) http://dx.doi.org/10.1016/j.fusengdes.2025.115052.
[20] J. Peric, D. Kotnik, D. Govekar, L. Snoj, V. Radulović, Validating a simplified water-activation transport model using time-resolved reactor-pulse neutron measurements at KATANA, Nucl. Eng. Technol. 58 (4) (2026) 104090, http://dx.doi.org/10.1016/j.net.2025.104090.
[21] U. Fischer, C. Bachmann, J. Catalan, T. Eade, D. Flammini, M. Gilbert, J.-C. Jaboulay, A. Konobeev, D. Leichtle, L. Lu, F. Malouch, F. Moro, P. Pereslavtsev, Y. Qiu, J. Sanz, P. Sauvan, G. Stankunas, A. Travleev, A. Turner, F. Ogando, I. Palermo, R. Villari, Methodological approach for DEMO neutronics in the European PPPT programme: Tools, data and analyses, Fusion Eng. Des. 123 (2017) 26–31, http://dx.doi.org/10.1016/j.fusengdes.2017.01.053, Proceedings of the 29th Symposium on Fusion Technology (SOFT-29) Prague, Czech Republic, September 5-9, 2016.

[22] Ž. Štancar, L. Snoj, An improved thermal power calibration method at the TRIGA mark II research reactor, Nucl. Eng. Des. 325 (2017) 78–89, http://dx.doi.org/10.1016/j.nucengdes.2017.10.020.

[23] G. Žerovnik, L. Snoj, et al., Measurements of thermal power at the TRIGA mark II reactor in Ljubljana using multiple detectors, IEEE Trans. Nucl. Sci. 61 (5) (2014) 2941–2948, http://dx.doi.org/10.1109/TNS.2014.2351774.

[24] The OpenFO.A.M. Foundation, Openfoam, 2025, https://openfoam.org/. (Accessed 5 April 2025).

[25] M.E. Rising, J. Armstrong, S. Bolding, F. Brown, J. Bull, T. Burke, A. Clark, D. Dixon, R. Forster III, J. Giron, et al., Mcnp® code version 6.3. 0 release notes, Los Alamos Natl. Lab. Los Alamos, NM, USA, Tech. Rep. la-UR-22-33103, Rev 1 (2023) 52.

[26] S.W. Mosher, S.C. Wilson, Algorithmic improvements to MCNP5 for high-resolution fusion neutronics analyses, Fusion Sci. Technol. 74 (4) (2018) 263–276.

[27] J. Wagner, Advantg–An automated variance reduction parameter generator, 2013.

[28] D. Brown, M. Chadwick, R. Capote, A. Kahler, A. Trkov, M. Herman, A. Sonzogni, Y. Danon, A. Carlson, M. Dunn, D. Smith, G. Hale, G. Arbanas, R. Arcilla, C. Bates, B. Beck, B. Becker, F. Brown, R. Casperson, J. Conlin, et al., ENDF/B-VIII.0: the 8th major release of the nuclear reaction data library with CIELO-project cross sections, new standards and thermal scattering data, Nucl. Data Sheets 148 (2018) 1–142, http://dx.doi.org/10.1016/j.nds.2018.02.001, Special Issue on Nuclear Reaction Data.

[29] R. Forrest, R. Capote, N. Otsuka, T. Kawano, A. Koning, S. Kunieda, J.-C. Sublet, Y. Watanabe, FENDL-3 Library-Summary Documentation, Tech. rep., International Atomic Energy Agency, 2012.

[30] J. García, J.P. Catalán, J. Sanz, Development of the automatic void generation module in GEOUNED conversion tool, Fusion Eng. Des. 168 (2021) 112366.